48th AIAA Aerospace Sciences Meeting Including the New Horizons Forum and Aerospace Exposition
4 - 7 January 2010, Orlando, Florida
AIAA 2010-820

A Hybrid Particle Scheme for Simulating Multiscale Gas Flows with Internal Energy Nonequilibrium

Jonathan M. Burt[1] and Iain D. Boyd [2]
Department of Aerospace Engineering
University of Michigan, Ann Arbor, MI 48109

A hybrid particle scheme, which is based on the direct simulation Monte Carlo (DSMC) method and incorporates a low diffusion particle method for continuum flow simulation, is extended for improved efficiency and wider applicability. The hybrid scheme is intended for simulation of gas flows involving a wide range of Knudsen number regimes, where strong coupling is desired between calculations in rarefied and continuum flowfield regions. A series of modifications are presented for cell-based numerical weight and time step adaptation, diffusive transport of nonequilibrium internal energy modes, and decreased sensitivity to DSMC cell size. Proposed modifications are employed in a hybrid simulation of a Mach 20 flow around a cylinder with a global Knudsen number of 0.002, for which a factor of 2.6 efficiency increase relative to full DSMC computation is demonstrated.

I. Introduction

In a variety of gas flow problems, portions of the flowfield exhibit large translational nonequilibrium effects and require relatively expensive simulation techniques based on the Boltzmann equation, while other regions are within low Knudsen number (*Kn*) continuum flow regimes and can be prohibitively expensive to simulate using such Boltzmann equation techniques. These "multiscale" flow problems include flows around atmospheric entry vehicles and hypersonic aircraft, where local *Kn* values based on gradient length scales may be very small through much of the flowfield but become large within shock, forebody boundary layer and wake regions. Other examples include rocket exhaust plumes and fuel venting flows at high altitude, where the mean free path may differ by several orders of magnitude between nearfield and farfield regions.

A. Simulation Methods for Multiscale Gas Flows

Accurate simulations may be performed for some of these flows using a two step, one-way coupled approach.[1-3] In this type of approach, continuum and rarefied regions are considered independently and different simulation techniques are applied in each region. In general, however, effects of two-way coupling between rarefied and continuum regions must be considered, and a single simulation employing a coupled hybrid algorithm is required. In one popular type of hybrid algorithm, a computational fluid dynamics (CFD) technique based on the Navier-Stokes equations is used in low-*Kn* continuum regions, the direct simulation Monte Carlo (DSMC) method is employed in rarefied regions, and additional procedures are used for evaluation of continuum breakdown and two-way information transfer between CFD and DSMC calculations.[4-9] Hybrid CFD-DSMC schemes have been the subject of considerable research over the past several years, and hybrid code development remains a topic of active research.

Other hybrid schemes for the same class of flows have also received some attention in recent years. In one scheme, a Navier-Stokes solver is coupled with deterministic solution methods for the Boltzmann equation.[10-12] This approach resolves the problem of statistical noise during information transfer from DSMC to CFD in a hybrid CFD-DSMC scheme, but introduces additional problems associated with grid selection in velocity space for the Boltzmann solver. This scheme may therefore be considerably more efficient than hybrid CFD-DSMC for many low Mach number (*M*) simulations where the DSMC noise problem is particularly severe, but is potentially more computationally expensive than CFD-DSMC schemes in high-*M* cases where a very large grid in velocity space would be required.

In another type of approach, DSMC-based low-*Kn* particle methods, such as a DSMC collision limiter scheme, are used in continuum regions, while standard DSMC is employed in rarefied regions.[13-17] This "all-particle"

[1] Post-doctoral research fellow, AIAA member.
[2] Professor, AIAA associate fellow.

approach is typically far easier to implement than a hybrid CFD-DSMC algorithm, and allows simple two-way information transfer across continuum breakdown boundaries without complicated coupling procedures as required for hybrid CFD-DSMC. As a further advantage of this last type of approach, similar procedures for rotational-translational and vibrational-translational energy exchange may be used within both rarefied and continuum regions.[18] Arbitrary levels of nonequilibrium in rotational and vibrational distribution functions are permitted in both regions, and no information regarding these distribution functions is lost during information transfer between continuum and rarefied domains. Similar or identical modeling procedures can also be used in both continuum and rarefied regions for additional physical phenomena, such as chemical reactions, particulate phases, and gas radiation.

Despite the above potential advantages of a particle-based hybrid approach, this type of hybrid algorithm has received relatively little attention in the literature, presumably due in part to large inherent numerical diffusion effects in DSMC collision limiter schemes and other DSMC-based low-*Kn* methods.[13,19] When the cell size is much larger than the local mean free path – as is typically required for simulation of low-*Kn* regions with comparable efficiency to CFD – these methods tend to produce very large numerical transport coefficients, with large associated numerical diffusion and dissipation errors in the presence of transverse gradients. As a result, DSMC-based hybrid particle techniques cannot offer the same favorable balance of efficiency and accuracy as hybrid CFD-DSMC for multiscale flow simulations involving low-*Kn* boundary layers, shear layers, slip lines or similar phenomena.

B. Low Diffusion Particle Method

As part of an alternative approach for hybrid simulation of multiscale flows involving a wide range of *Kn* regimes, a DSMC-based low diffusion (LD) particle method has recently been developed by the authors.[20,21] This new method avoids the numerical diffusion problems inherent in other DSMC-based low-*Kn* schemes, and should be comparable to explicit CFD schemes in both accuracy and efficiency for simulating low-*Kn* flow phenomena such as continuum boundary layers, free shear layers, slip lines, and contact discontinuities. When used as part of a hybrid algorithm with DSMC, this scheme offers similar benefits in simplicity and ease of implementation as other DSMC-based low-*Kn* particle methods, without the drawbacks of reduced accuracy when cell and time step sizes are much larger than allowed by DSMC.[22,23]

In recent work, a hybrid scheme utilizing the LD particle method has been extended to include rotational and vibrational nonequilibrium effects, for consistent treatment of internal energy modes in both continuum and rarefied regions.[24] In a series of homogeneous relaxation problems, capabilities for nonequilibrium rotational and vibrational energy distributions were demonstrated, and good agreement with DSMC was shown for time variation in quantized vibrational energy level populations. As with other DSMC-based hybrid particle schemes, the LD-DSMC scheme avoids any loss of information regarding nonequilibrium internal energy distributions along continuum breakdown boundaries. This should make the LD-DSMC scheme ideal for simulating multiscale flows which involve significant vibrational or rotational nonequilibrium effects within both continuum and rarefied regions. However, previous test cases have been limited to homogeneous flows and multidimensional flows without boundary layers or strong transverse gradients, due to a lack of capabilities for modeling diffusive transport of internal energy modes. As an additional limitation of previous test cases, no efficiency gains relative to DSMC were realized in a hypersonic blunt body flow problem, due to a lack of variation between continuum and rarefied regions in both time step and the number of particles per unit volume.

C. Outline of the Paper

In this paper, both diffusive energy transport and efficiency issues in hybrid LD-DSMC simulations are addressed. First, procedures are described for inclusion of diffusive internal energy transport in the LD particle method. These procedures involve a finite volume solution to the diffusive portion of the vibrational energy transport equation, with temperature gradient terms computed using time averages to reduce statistical scatter. Vibrational energy is added or removed from each LD cell during each simulation time step through an energy rescaling procedure, while diffusive rotational energy transport is modeled more simply by assuming rapid accommodation to the local translational temperature.

Next, procedures are described for automatic particle weight and time step assignment, in order to increase hybrid simulation efficiency relative to DSMC. For this increase in efficiency, the cell size requirements are relaxed in comparison to standard DSMC guidelines, so that cells throughout the computational mesh can be larger than the local mean free path. When a cell is assigned to DSMC during periodic domain decomposition routines, the cell-based time step interval is reduced to some fraction of the local mean collision time, and the cell is divided into a number of subcells for use in nearest-neighbor DSMC collision partner selection. Numerical weight values in DSMC regions are also reduced to assure an adequate particle population within each subcell. Thus, while no dynamic mesh adaptation is performed, DSMC requirements for time step size and mean collision separation are

automatically met. As an additional modification to DSMC for use with large cells, binary collision probabilities are adjusted using a linear reconstruction scheme to compensate for density variation within a cell. The use of larger time steps and fewer particles per cell in continuum regions should allow for efficiency increases relative to DSMC in a hybrid LD-DSMC simulation. Such efficiency increases are demonstrated for a representative test case involving a flow of vibrationally excited N_2 around a cylinder with a global Knudsen number (based on cylinder diameter) of 0.002 and a freestream Mach number of 20.

II. Modifications for Diffusive Internal Energy Transport

Simulation procedures in the LD particle method are described in detail in Refs. 20-24, and the reader is referred to these papers for a discussion of procedures, assumptions, and efficiency considerations in the method. Reference 20 describes the basic LD method for simulation of inviscid compressible gas flows. Reference 21 outlines modifications to the LD method for application to viscous flows within the same *Kn* range as the compressible Navier-Stokes equations. In Ref. 22, procedures are described for strong two-way coupling between LD and DSMC calculations in a hybrid code. Further modifications are proposed in Ref. 23 for simulating flows involving viscous transport in a gas mixture. Reference 24 includes descriptions of two separate models for inclusion of nonequilibrium internal energy distributions, with probabilistic energy exchange procedures that allow good agreement with DSMC relaxation rates and avoid information loss along LD-DSMC domain boundaries in a hybrid simulation.

As discussed in the introduction, internal energy nonequilibrium capabilities presented in Ref. 24 do not consider diffusive internal energy transport. Without the addition of a model for this transport process, nonphysical transverse gradients or discontinuities can exist in vibrational or rotational temperature (as found along LD-DSMC domain boundaries within the forebody boundary layer in a hybrid simulation of a hypersonic blunt body flow) and viscous flow routines outlined in Ref. 21 must be disabled to avoid these problems. Thus, to take advantage of both viscous flow simulation capabilities and internal energy nonequilibrium in LD method calculations, new procedures must be added to account for diffusive transport of rotational and vibrational energy. These procedures are presented as follows.

A. Vibrational Energy

For inclusion of vibrational energy diffusive transport, a value for vibrational temperature T_v is included in the cell data structure and is stored separately for every cell. During each simulation time step, T_v values are updated using an exponential moving average[25] to reduce scatter relative to instantaneous cell-based temperatures. For a simple (one species) diatomic gas with vibrational excitation, this temperature is computed as

$$T_v = (1-\alpha)T_v^* + \frac{\alpha\,\theta_v}{\ln\left(1+k_B\theta_v/\langle e_v\rangle\right)} \tag{1}$$

where the superscript "*" denotes the cell T_v value during the previous time step, k_B is Boltzmann's constant, $\langle e_v\rangle$ is the average vibrational energy among all particles in the cell during the current time step, θ_v is the characteristic vibrational temperature for the gas species, and α is a relaxation parameter between zero and one. An α value of 0.01 is used in this work, and seems to give a reasonably good balance of scatter reduction and low time lag for T_v relative to instantaneous cell-based vibrational temperature values.

Once the temperature T_v has been updated for all cells during the current time step, a finite volume procedure is used to determine the total vibrational energy ΔE_v which must be added to each cell over the time step interval Δt to account for diffusive transport. Following Ref. 21, a summation is performed over all faces *f* for a given cell:

$$\Delta E_v = \Delta t \sum_{f=1}^{N_f} A_f \left(k_v\right)_f \left(\frac{\partial T_v}{\partial n}\right)_f \tag{2}$$

Here N_f is the total number of cell faces, A_f is the face area, $(k_v)_f$ is an unweighted average of vibrational thermal conductivity values for cells on either side of a face, and $(\partial T_v/\partial n)_f$ denotes the normal gradient in T_v along the face. In a first order implementation, $(\partial T_v/\partial n)_f$ may be calculated as the difference between T_v values for the two neighboring cells at face *f*, divided by the face-normal projection of the vector between the two cell centers. The

vibrational thermal conductivity k_v is evaluated for each cell through Eucken's relation,[26] as a function of the dynamic viscosity μ and molecular mass m:

$$k_v = \frac{\mu k_B}{m} \frac{\theta_v / T_v}{\exp(\theta_v / T_v) - 1} \tag{3}$$

For consistency with DSMC in a hybrid simulation, μ may be calculated using either the variable hard sphere collision model, as in Ref. 21, or the variable soft sphere model as in Ref. 23.

Once ΔE_v has been computed for a given cell, particle vibrational energy values in this cell must be modified to account for the addition or removal of energy. As a simple means of enforcing energy conservation, all particle vibrational energy values e_v are multiplied by a factor F_v

$$F_v = 1 + \frac{\Delta E_v}{W\left(\Delta t / \Delta t_{ref}\right) N_p \left\langle e_v \right\rangle} \tag{4}$$

where W is the cell numerical weight (i.e. the number of gas molecules represented by each particle in the cell), Δt_{ref} is a global reference time step, and N_p is the current number of particles in the cell.

While the procedure involving Eqs. (1) through (4) is relatively efficient and simple to implement, it should be noted that this procedure permits vibrational energy values outside the quantum levels $k_B \theta_v i$ allowed by the simple harmonic oscillator (SHO) model[26] used for LD method calculations in Ref. 24. Moreover, this procedure does not distinguish between diffusion processes for individual vibrational energy levels, as occurs in diffusive transport associated with Brownian motion of DSMC particles or real molecules in the gas. To include these quantum effects, two alternative diffusive transport schemes which allow only quantized SHO energy levels have also been implemented and tested. (One scheme rounds each e_v value to the nearest quantum level, then adds the cumulative rounding error to the ΔE_v value used in the same cell during the next time step. In another scheme, e_v values are increased or decreased by a single quantum level for as many randomly selected particles in the cell as necessary, and any small remaining portion of ΔE_v is carried over to the next time step.) However, the added complexity in quantized transport procedures does not seem to provide significant improvements in accuracy for a representative test case, and the non-quantized procedure described above is assumed to be sufficiently accurate for most applications. For post-processing determination of quantized vibrational energy distributions in a simulation employing Eqs. (1) through (4), e_v values may be rounded to the nearest quantum level.

B. Rotational Energy

To model diffusive transport of rotational energy, a similar procedure to that involving Eqs. (1) through (4) can be used, with rotational thermal conductivity equal to $\mu k_B / m$ for a simple diatomic gas. However, a much simpler treatment of this transport process may be used under conditions where characteristic time scales for rotational energy diffusion are much larger than those for rotational-translational energy exchange. This assumption is generally valid in the low-Kn flow regimes for which the LD method is appropriate, due to high collision frequencies and a small rotational collision number. Under such conditions, both translational and rotational components of the thermal conductivity (together equal to $4.75 \mu k_B / m$ for a simple diatomic gas) should be used to update particle temperatures during each time step, as described in Ref. 21. Rotational-translational energy exchange procedures outlined in Ref. 24 then allow rapid equilibration of the rotational energy distribution to the local translational temperature, and no further procedures are required for consideration of rotational energy diffusive transport.

III. Modifications for Improved Hybrid Simulation Efficiency

As discussed in the introduction, previous hybrid LD-DSMC simulations of hypersonic blunt body flows did not show any efficiency improvements over simulations performed using only DSMC.[22,24] This can be attributed to a lack of cell and time step adaptation in continuum regions; while the LD particle method allows for potentially much larger cells and time step intervals than are typically used in DSMC, previous LD-DSMC hypersonic flow simulations did not take advantage of this, and instead used sufficiently small cells and time step values to meet standard DSMC guidelines within both DSMC and LD domains. In contrast, the current work should allow hybrid efficiency gains relative to DSMC through a combination of automatic time step adaptation, DSMC subcells for

nearest neighbor collision selection, modifications to the DSMC collision probability for large cells, and numerical weight adaptation to reduce particle populations in continuum regions.

A. Subcells for DSMC Collision Calculations

For the desired efficiency increase, hybrid simulations are performed on a mesh which is sufficiently refined for mesh independence in LD calculations, but is considerably less refined than necessary to meet DSMC guidelines.[27] During collision selection routines as part of DSMC calculations, each cell in the DSMC domain is divided into a number of subcells, with subcell dimensions set to approximately half the local mean free path. Collision partners are then selected from particles located in either the same subcell or neighboring subcells. Provided sufficient particle populations exist within each subcell, the use of subcells should reduce or eliminate any dependence of mean collision separation on DSMC cell size.

B. Continuum Breakdown Evaluation

In the present work, domain decomposition calculations are performed once every 2000 time steps, at which time all cells are assigned to either DSMC or LD domains based on evaluations of a gradient-based continuum breakdown parameter.[21] Given the local hard sphere mean free path λ,[27] cells are assigned to the DSMC domain if the condition

$$\frac{\lambda}{Q}\left|\nabla Q\right| > 0.05 \tag{5}$$

is satisfied for Q equal to any scalar flowfield quantity among a list that includes the time-averaged bulk gas speed, density and translational temperature. (For Q equal to the bulk gas speed, the left side of (5) is multiplied by the ratio of the bulk speed to the local speed of sound, in order to improve accuracy for continuum breakdown evaluations in subsonic regions.) Following initial cell assignment, a smoothing operation is used to reduce the surface area along LD-DSMC domain boundaries, and two layers of buffer cells – each three cells thick – are identified along these boundaries.[22]

C. Numerical Weight and Time Step Adaptation

Immediately after domain decomposition routines, additional procedures are run to optimize time step Δt and numerical weight W values for each cell. As a first step in these optimization procedures for a given cell, the time step interval is updated from the value Δt^* used in this cell during the previous 2000 time steps to a new value Δt. In cells within the LD domain, Δt is calculated to give a desired Courant number[28] of 0.2, while in DSMC cells the time step size is set to 0.2 times the local mean collision time. Next, the minimum desired number of particles N_d is determined for this cell. In the LD domain a uniform N_d value of 20 is used, while in DSMC cells N_d varies as a function of the ratio of cell size to the mean free path, in order to fix the expected number of particles per subcell. Here we use $N_d = 3N_s$, where N_s is the number of subcell divisions for a given cell during the current time step. For a two-dimensional cell with a subcell size of approximately $\frac{1}{2}\lambda$, this corresponds to a desired number of 12 particles per square mean free path.

Once both Δt and N_d have been determined for a given cell, the cell numerical weight W is updated from the value W^* employed during the previous 2000 time steps. The new weight must be a power of two, and is set such that the expected number of particles in the cell is between N_d and $2N_d$. This new weight is calculated as $W = 2^p$ where p is an integer given by

$$p = \left\lfloor \frac{1}{\ln(2)} \ln\left(W^* \frac{\langle N_p \rangle \Delta t^*}{N_d \Delta t} \right) \right\rfloor \tag{6}$$

Here the operator $\lfloor\ \rfloor$ rounds to the nearest smaller integer, and $\langle N_p \rangle$ is the time-averaged number of particles in the cell. A smoothing operation, similar to that employed for LD/DSMC cell assignments,[22] may be used to provide more uniform integer values for p among nearby cells. After new Δt and W values have been assigned to a cell, all particles in the cell are considered for cloning if $W\Delta t < W^*\Delta t^*$, or for removal if $W\Delta t > W^*\Delta t^*$. Particles are cloned or removed, as described by Bird[27] to correct for cell-based variations in numerical weight, so that the current number

of particles N_p in the cell will change on average by the factor $W^*\Delta t^*/W\Delta t$. Time-averaged quantities (such as T_v and $\langle N_p \rangle$) stored in the cell data structure are multiplied by this same factor.

The above procedures are intended to allow for appropriate Δt and W assignment within the LD domain, while enforcing DSMC requirements for time step and mean collision separation in the DSMC domain. Far more particles may be located in each DSMC cell than in each LD cell, and the primary means of hybrid efficiency gains relative to DSMC will be through large reductions in the particle population within continuum regions.

It should be noted that some unavoidable accuracy loss will result from the spatial variation in numerical weight, as some particles must be cloned or destroyed when they pass between neighboring cells with different W values. However, this accuracy loss should be reduced here through three different means: First, numerical weight values W are restricted to powers of two. Every particle that moves into a new cell with a W value one-half that of the previous cell will be cloned, while any particle moving in the opposite direction between the same two cells has a 50% probability of removal. In this case mass, momentum and energy are all exactly conserved during cloning, whereas conservation occurs only in an average sense during removal and some associated random walk error is expected. In a second mechanism for error reduction, the above procedures tend to produce large regions of the mesh within which all cells are assigned the same W value. This dramatically reduces the frequency of particle cloning and removal, which should in turn reduce the errors associated with these processes. Lastly, as is standard practice in DSMC, buffers are used to delay the introduction of clone particles.[27] Each newly generated clone particle is placed in a cell-based linked buffer list for the following ten time steps, before being released and allowed to participate in move and collide operations. As a result, any effects of particle cloning on gas velocity distributions and DSMC collision partner selection should be reduced.

D. Modification to DSMC Collision Probabilities

One final modification is needed to compensate for the reduction in accuracy associated with using DSMC cells larger than the local mean free path. Note first that the use of dynamically adaptive subcells, as described above, allows mean collision separation values which have little or no dependence on the ratio of cell size to mean free path. Within very large cells however, substantial variation may exist in the local time-averaged number density. This in turn can lead to reduced accuracy in collision probability calculations, as illustrated through the following logic.

The no time counter (NTC) collision selection scheme[27] is typically used in DSMC to calculate the total number of potential collision pairs in the cell, after which collision probabilities for individual pairs are evaluated without regard to location in the cell. Here the total number of pairs is proportional to $N_p\langle N_p \rangle/V$ (or equivalently $N_p(N_p-1)/V$) where V is the cell volume. These procedures are based on an assumption that the time-averaged number of particles per unit volume is spatially homogeneous within the cell. Under this assumption, the average particle density at any point in the cell is approximated by $\langle N_p \rangle/V$. As an extreme example of the resulting inaccuracy in very large cells, consider a case where all particles are consistently located within one half of the cell volume. This means that the particle density within the occupied portion of the cell is $2\langle N_p \rangle/V$, and the NTC scheme will underestimate collision probabilities on average by a factor of two.

To compensate for this error in collision probabilities when a DSMC cell is significantly larger than the mean free path, we multiply the collision probability for each potential collision pair by the ratio n_{ij}/n_c, where n_{ij} is an estimate of the gas number density at the collision center of mass, n_c is the cell-averaged number density, and i and j are indices for the two particles. Using a linear reconstruction of the number density at any point in the cell, we can express this ratio as

$$\frac{n_{ij}}{n_c} = 1 + \frac{1}{n_c}\left(\nabla n\right)_c \cdot \left(\frac{m_i \boldsymbol{x}_i + m_j \boldsymbol{x}_j}{m_i + m_j} - \boldsymbol{x}_c \right) \tag{7}$$

where m_i and $\boldsymbol{x}_i$ are respectively the mass and location of particle i, and $\boldsymbol{x}_c$ is the cell center location. Other terms in Eq. (7) are calculated as follows:

$$\begin{aligned} n_c &= \frac{W\left(\Delta t/\Delta t_{ref}\right)\left\langle N_p \right\rangle}{V} \\ \left(\nabla n\right)_c &= \frac{1}{V}\sum_{f=1}^{N_f} A_f n_f \mathbf{n}_f \end{aligned} \tag{8}$$

Here n_f is the number density along a cell face f with an outward normal unit vector $\mathbf{n}_f$. Each face density value n_f is computed as the unweighted average of cell values n_c for the cells on either side of the face. Note that the linear reconstruction implied in (7) is monotonicity preserving, and only allows n_{ij} values within a range bounded by the cell-averaged number densities n_c for neighboring cells.

As employed in the current work, DSMC collision probabilities are first calculated using the standard NTC scheme, after which these probabilities are multiplied by n_{ij}/n_c in any cell with dimensions larger than two times the local mean free path. While this added procedure should have some effect on overall DSMC simulation expense, initial tests indicate an efficiency reduction of less than 2%. Further work is required to evaluate the accuracy and limitations of this procedure. However, we find no noticeable accuracy loss when Eq. (7) is applied to cells which meet standard DSMC guidelines, and it seems reasonable to assume that this procedure allows some reduction in spatial discretization errors when larger cells (e.g. between two and five mean free paths in length) are used.

IV. Application to a Hypersonic Blunt Body Flow

Hybrid LD-DSMC simulation procedures outlined above are applied to a representative multiscale flow of vibrationally excited N_2 over a cylinder. The global Knudsen number based on cylinder diameter is 0.002, the freestream Mach number is 20, the freestream temperature is 217.5 K, and the cylinder surface is modeled as a diffusely reflecting wall at a temperature of 1500 K.

A. Simulation Setup

Calculations using the LD particle method, as performed in continuum flowfield regions, involve the "LD1" scheme for probabilistic vibrational-translational and rotational-translational energy exchange described in Ref. 24. Both DSMC collision calculations and viscous transport calculations in the LD method employ the variable hard sphere model.[27] To reduce the size of small pressure discontinuities (corresponding to an error of around 1%) observed along LD/DSMC domain boundaries, all "LD-type" particles in the buffer region adjacent to the LD domain are randomly repositioned within the assigned cells during each time step. As discussed in Ref. 20, other particles in the LD domain are randomly repositioned an average of once every 10 time steps.

The simulation is performed on a structured mesh, as shown in Fig. 1, which consists of 45,000 quadrilateral cells ranging in size from around 0.5 to 5 times the local mean free path at steady state. At simulation startup, the flowfield is initialized with uniform ambient conditions, and all cells are initially assigned to the DSMC domain. LD/DSMC domain assignments, numerical weight values and time step scaling factors are subsequently updated in each cell once every 2000 time steps. Steady state conditions are assumed following a transient period of 60,000 steps, after which 40,000 additional steps are used for sampling.

B. Efficiency Considerations

The hybrid LD-DSMC simulation is performed in parallel, on 16 processors in the nyx cluster at the University of Michigan. For comparison, a standard DSMC simulation for this flow is also performed, with identical models and numerical parameters as those employed in DSMC calculations in the hybrid simulation. Total CPU times are approximately 196 hours for the hybrid LD-DSMC simulation and 508 hours for the DSMC simulation. Thus, hybrid procedures allow a reduction in overall simulation expense by a factor of about 2.6 relative to DSMC. The hybrid LD-DSMC approach also allows a large reduction in the total number of simulated particles; at steady state, roughly 2.9 million particles are used in the hybrid simulation while around 13.1 million particles are used in the DSMC simulation. (Of the 2.9 million particles in the hybrid simulation, approximately 300,000 are assigned to about 10,400 cells within the LD domain. The corresponding region in the DSMC simulation is estimated to include around 10.5 million particles at steady state.)

Note that the relative hybrid simulation efficiency is found to further increase when the global Knudsen number is reduced, and that any speedup associated with a potentially smaller number of time steps during the transient period is not considered here. Several additional changes, which are not employed here, would also increase the relative efficiency of the hybrid simulation: A smaller number of processors could be used in the LD-DSMC simulation than in the DSMC simulation, so that a comparable number of particles would be assigned to each processor in both simulations, and parallel communication losses in the LD-DSMC simulation would be reduced. Parallel efficiency could also be improved by accounting for the difference (by a factor of roughly 1.5) in average computational expense per particle per time step during automated procedures for parallel domain decomposition.[20] In a further modification for improved hybrid simulation efficiency, the DSMC region surrounding the shock could conceivably be narrowed or eliminated. This reduction in size of the DSMC domain may be justified by the fact that

accurate characterization of the shock structure (which requires that DSMC be used within the shock) tends to have little influence on boundary layer and surface properties for this type of flow. Finally, automatic time step and weight adaptation routines could be disabled in DSMC calculations, so that a uniform numerical weight and time step size would be used over the full DSMC domain. This would dramatically increase DSMC simulation expense, and show a large increase in the relative efficiency of the hybrid LD-DSMC simulation.

C. Simulation Results and Comparison with DSMC

Figure 2 shows streamlines and LD/DSMC domain boundaries at steady state from the hybrid simulation, with corresponding streamlines from the DSMC simulation in the lower half of the figure. As expected, rarefied regions assigned to the DSMC domain in the hybrid simulation include a narrow region surrounding the bow shock, the near-wall portion of the forebody boundary layer, and much of the wake. Very good agreement is found between streamlines from the two simulations, with little noticeable difference in location of the bow shock or in the size and position of the recirculating region behind the cylinder. Accurate representation of the recirculating region is generally a good indicator of overall simulation accuracy for this type of flow, so the very good agreement observed here is encouraging.

In Figs. 3, 4 and 5, iso-contour lines are shown for translational, rotational and vibrational temperature, respectively, from both the hybrid LD-DSMC and DSMC simulations. Hybrid simulation results are displayed as solid multicolored lines, while dashed red lines indicate DSMC results. LD/DSMC domain boundaries in the hybrid simulation are also shown in the figures. Good overall agreement is found between the two simulations for all three temperatures, with maximum disagreement observed in the recirculating wake region just downstream of the cylinder. Within this region, we find that the hybrid simulation gives a maximum overestimate in both translational and rotational temperatures of about 6%, with a corresponding overestimate of around 9% in vibrational temperature. While the magnitude of these discrepancies may seem discouraging, it should be emphasized that accurate temperature determination within such recirculating regions can be difficult due to relative isolation from the surrounding flowfield. (Errors in hybrid simulation results within the recirculating region are likely affected by by the fact that a small number of cells in this region are assigned to the LD domain. These errors could potentially be reduced by reassigning such cells to the DSMC domain, through either manual user intervention or an increased level of smoothing for continuum breakdown boundaries.) Outside of the recirculating region and the area of large temperature gradients around the shock, the maximum disagreement in all three temperatures is in the range of 4–5%.

Figure 6 shows the variation in translational, rotational and vibrational temperatures from both simulations along the stagnation streamline. Vertical lines in the figure denote LD/DSMC domain boundaries in the hybrid simulation. Very good overall agreement is observed between the two sets of results, with nearly identical translational temperature spikes in the shock and only a slight overestimate in shock standoff distance in the hybrid simulation. Small but noticeable statistical scatter is found in the temperature curves, with the most pronounced scatter within the plateau region between the shock and boundary layer. Differences between results from the two simulations are greatest near the outer portion of the boundary layer, where temperatures are consistently underestimated in the hybrid simulation by around 3%. Note the lack of slope discontinuities or spikes along LD/DSMC boundaries in the hybrid simulation results, which indicates consistency in diffusive energy transport between DSMC and LD method calculations.

In Fig. 7, the gas density and bulk velocity magnitude are plotted as a function of distance from the wall along the stagnation streamline. As in Fig. 8, good overall agreement is observed, with only very small differences in both shock standoff distance and shock thickness. Maximum velocity and density gradients within the shock are nearly identical, and good agreement is also observed in the density variation within the boundary layer. As one indicator of the level of agreement between the two density profiles, the stagnation point density is overestimated in the hybrid simulation by approximately 3% relative to the DSMC simulation result.

Figure 8 shows the variation in translational, rotational and vibrational temperatures along an extraction line which passes through the cylinder center and is inclined 60° from the direction of freestream flow. Similar trends are observed in Fig. 8 as in Fig. 6, with maximum relative errors in translational and rotational temperatures of around 2%. A maximum relative error in vibrational temperature of around 11% is found near the LD/DSMC domain boundary at the downstream edge of the shock. While the significance of this discrepancy should not be overlooked, the absolute difference in vibrational temperature at this location is about 180 K, which is not much larger than the maximum absolute differences in either translational or rotational temperature. The corresponding variation in bulk velocity magnitude and density along the same extraction line is shown in Fig. 9. Very good agreement is found here in both quantities, with comparable errors in the hybrid simulation to those observed for the same quantities in Fig. 7.

Figure 10 shows the variation along the stagnation streamline in the fraction of N_2 molecules at the first excited quantum vibrational level, as calculated from both LD-DSMC and DSMC simulations. In an additional curve labeled "LD-DSMC*", results are plotted from a hybrid simulation for which the desired number of particles in the LD domain is increased from 20 to 40. Measured in average CPU time per time step, this second LD-DSMC simulation is approximately 30% more expensive than the first, and gives a factor of 2.0 reduction in simulation expense relative to DSMC. For both LD-DSMC curves in Fig. 10, the number of sampling time steps is increased from 40,000 – as used for results displayed in Figs. 1 through 9 – to 100,000, in order to further reduce statistical scatter. Note that the level of scatter in this quantity is particularly high within the LD domain, due to the comparatively small number of particles per cell. For comparison, the figure also shows the corresponding excited fraction based on the equilibrium Boltzmann distribution at the local vibrational temperature from the LD-DSMC simulation.

While considerable scatter is observed in both LD-DSMC and DSMC results in Fig. 10, we do find reasonably good overall agreement between results from the different simulations. In both types of simulations, the fraction of excited molecules rises from zero to around 0.16 in the downstream portion of the shock, then levels off before rising slightly in the boundary layer and dropping down to approximately 0.12 at the relatively cold wall. The one region of relatively poor agreement is in the downstream portion of the post-shock LD area, where DSMC simulation values are up to 10% greater than those from the hybrid LD-DSMC simulation with 20 desired particles per cell. Some of the discrepancy here is likely due to the unphysical nature of vibrational energy rescaling, as part of procedures outlined in section II-A to account for diffusive vibrational energy transport. Additional error in hybrid results may be caused by the use of different mechanisms for vibrational-translational energy exchange in LD and DSMC calculations as part of the hybrid simulation. The reader is referred to Ref. 24 for a detailed discussion of the differences between "LD1" and DSMC energy exchange approaches which are used in these simulations.

While both diffusive transport and energy exchange calculations may contribute to differences observed in Fig. 10, most of the accuracy loss in hybrid simulation results is likely associated with the small number of LD-type particles per cell within the post-shock region. This conclusion is based on the fact that significantly better agreement is found here between curves labeled DSMC and LD-DSMC* than between DSMC and LD-DSMC curves. The maximum discrepancy in Fig. 10 between values from the DSMC simulation and from the LD-DSMC simulation with 40 desired particles per cell is around 3.4%, which is one-third that of the hybrid simulation with fewer particles per cell. Dependence on the number of particles per cell is likely a result of calculating the instantaneous vibrational temperature, which is proportional to the second term on the right side of Eq. (1), as a function of vibrational energy values for only those particles currently located within a given cell. Note that this approximation does not seem to significantly affect vibrational temperatures, but can reduce accuracy in the calculated vibrational distribution function within regions of strong temperature gradients where relatively few particles are assigned to each cell. Thus, even better agreement with DSMC is expected in a hybrid simulation for which the desired number of particles per cell is larger than 40, and averaging the particle vibrational energy over multiple time steps in Eq. (1) may further reduce the error observed in hybrid results.

In contrast to DSMC and LD-DSMC simulation results plotted in Fig. 10, the excited fraction at equilibrium (labeled "Boltzmann" in the legend) is found to increase to around 0.25 within both the shock and boundary layer, and to approach 0.23 at the wall. Local maxima in the equilibrium curve within regions of progressively increasing and decreasing vibrational temperature (in the shock and boundary layer respectively) may be attributed to the following logic: As the vibrational temperature and level of vibrational excitation both increase from zero, the fraction at the first excited level initially increases as molecules transition from the ground energy level, after which this fraction begins to decrease due to increasing populations at higher energy levels.

In comparing the equilibrium curve in Fig. 10 with results from both LD-DSMC and DSMC simulations, we find relatively poor overall agreement. Note in particular the deviation from equilibrium in LD-DSMC and DSMC simulation values within the LD region just downstream of the shock. As mentioned above, significant differences are also found between DSMC and LD-DSMC results in Fig. 10, due to a combination of diffusive transport procedures in section II-A, the use of different techniques for vibrational-translational energy exchange, and error associated with the small number of particles per cell within the LD domain. Still, the lack of information loss related to quantum vibrational levels along continuum breakdown boundaries, and the preservation of nonequilibrium characteristics across these boundaries, can be seen as advantages of the hybrid LD-DSMC scheme in relation to coupled CFD-DSMC schemes. These capabilities should therefore provide a basis for implementation of additional models – such as radiative heat transfer or vibrationally favored dissociation – in the hybrid LD-DSMC code.

V. Summary and Conclusions

A strongly coupled hybrid particle scheme for simulation of multiscale flows involving a wide range of *Kn* regimes has been modified for improved efficiency and wider applicability. Modifications were proposed for diffusive transport of nonequilibrium internal energy, in order to permit simulation of flows involving both large transverse gradients and thermal nonequilibrium effects within continuum regions. Other procedures were outlined for automatic and dynamic adaptation of cell-based numerical weight and time step values. A series of modifications were also described for improving the accuracy of DSMC calculations, which are performed in high *Kn* regions as part of a hybrid simulation, when cells are out of range of standard DSMC guidelines.

As proposed here, sensitivity to DSMC cell size can be reduced through a combination of careful limitations on time step size, a decrease in mean collision separation via subcells and dynamic weight variation, and adjustments to collision probabilities. By allowing somewhat larger DSMC cells, we can increase hybrid simulation efficiency through the use of fewer particles per unit volume in continuum regions, while avoiding any complex procedures for adaptive mesh refinement as used in other DSMC-based hybrid schemes.[4,5] Note however that any increase in allowable DSMC cell size is not accompanied by a reduction in computational expense for DSMC calculations, as sufficient DSMC particle populations are still required to ensure that the mean collision separation is much smaller than the local mean free path. Additional work is required to verify and evaluate limitations of proposed modifications, particularly the adjustment to DSMC collision probabilities. Still, these modifications are employed in the present work using relatively conservative numerical parameters which should be well within the validity range for various underlying assumptions.

Newly proposed modifications to the hybrid LD-DSMC scheme have been applied to a hypersonic flow of vibrationally excited N_2 over a cylinder. A factor of 2.6 reduction in simulation expense relative to DSMC was demonstrated, and good overall agreement was observed with DSMC simulation results. The demonstrated efficiency gain may not provide sufficient motivation to use the hybrid LD-DSMC approach in place of DSMC, but it should be noted that the relative efficiency of the hybrid scheme should increase as the global Knudsen number is further reduced and larger portions of the flowfield are assigned to the LD domain. Moreover, the hybrid scheme should allow accurate simulation regardless of the *Kn* regimes involved. This potentially allows use of a single code, with a single set of numerical models, for flows around atmospheric entry or launch vehicles over the full flight trajectory.

Future work is expected to include more detailed accuracy and efficiency evaluations for realistic reentry type problems, with additional models for chemistry and/or other physical phenomena. Several of the proposed modifications mentioned in section IV-B will be implemented, in order to realize greater efficiency savings relative to DSMC. Additional work may involve application to high altitude rocket exhaust flows, as in Ref. 23. Analysis and testing of the proposed modifications to reduce DSMC cell size sensitivity is also planned.

Acknowledgments

The authors gratefully acknowledge NASA for financial support of this work, through grant NNX08AD02A.

References

[1]Papp, J. L., Wilmoth, R. G., Chartrand, C. C., and Dash, S. M., "Simulation of High-Altitude Plume Flow Fields Using A Hybrid Continuum CFD/DSMC Approach," AIAA Paper 2006-4412, 2006.

[2]VanGilder, D. B., Chartrand, C. C., Papp, J. L., Wilmoth, R. G., and Sinha, N., "Computational Modeling of Nearfield to Farfield Plume Expansion," AIAA Paper 2007-5704, 2007.

[3]Gimelshein, S. F., Levin, D. A., and Alexeenko, A. A., "Modeling of Chemically Reacting Flows from a Side Jet at High Altitudes," Journal of Spacecraft and Rockets, Vol. 41, No. 4, 2004, pp. 582-591.

[4]Schwartzentruber, T. E., and Boyd, I. D., "A Modular Particle-Continuum Numerical Method for Hypersonic Non-equilibrium Gas Flows," *Journal of Computational Physics*, Vol. 225, 2007, pp. 1159-1174.

[5]Lian, Y.-Y., Wu, J.-S., Cheng, G., and Koomullil, R., "Development of a Parallel Hybrid Method for the DSMC and NS Solver," AIAA Paper 2005-0435, 2005.

[6]Kaplan, C. R., Liu, J., and Oran, E. S., "Parallel Hybrid Method for Subsonic Flows: Coupling and Load-Balancing Challenges," AIAA Paper 2006-992, 2006.

[7]Garcia, A. L., Bell, J. B., Crutchfield, W. Y., and Alder, B. J., "Adaptive Mesh and Algorithm Refinement Using Direct Simulation Monte Carlo," *Journal of Computational Physics*, Vol. 154, 1999, pp. 134-155.

[8]Wadsworth, D. C., and Erwin, D. A., "Two-Dimensional Hybrid Continuum/Particle Approach for Rarefied Flows," AIAA Paper 92-2975, 1992.

[9]Hash, D. B., and Hassan, H. A., "Assessment of Schemes for Coupling Monte Carlo and Navier-Stokes Solution Methods," *Journal of Thermophysics and Heat Transfer*, Vol. 10, No. 2, 1996, pp. 242-249.
[10]Kolobov, V. I., Arslanbekov, R. R., Aristov, V. V., Frolova, A. A., and Zabelok, S. A., "Unified Solver for Rarefied and Continuum Flows with Adaptive Mesh and Algorithm Refinement," *Journal of Computational Physics*, Vol. 223, 2007, pp. 589-608.
[11]Kolobov, V. I., Bayyuk, S. A., Arslanbekov, R. R., Aristov, V. V., Frolova, A. A., and Zabelok, S. A., "Construction of a Unified Continuum/Kinetic Solver for Aerodynamic Problems," *Journal of Spacecraft and Rockets*, Vol. 42, No. 4, 2005, pp. 598-606.
[12]Josyula, E., Arslanbekov, R. R., Kolobov, V. I., and Gimelshein, S. F., "Evaluation of Kinetic/Continuum Solver for Hypersonic Nozzle-Plume Flow," *Journal of Spacecraft and Rockets*, Vol. 45, No. 4, 2008, pp. 665-676.
[13]Breuer, K. S., Piekos, E. S., and Gonzales, D. A., "DSMC Simulations of Continuum Flows," AIAA Paper 95-2088, 1995.
[14]Titov, E. V., Zeifman, M. I., and Levin, D. A., "Application of the Kinetic and Continuum Techniques to the Multi-Scale Flows in MEMS Devices," AIAA Paper 2005-1399, 2005.
[15]Pullin, D. I., "Direct Simulation Methods for Compressible Inviscid Ideal-Gas Flow," *Journal of Computational Physics*, Vol. 34, 1980, pp. 231-244.
[16]Macrossan, M. N., "A Particle-Only Hybrid Method for Near-Continuum Flows," *Rarefied Gas Dynamics: 22nd International Symposium*, American Institute of Physics, 2001, pp. 388-395.
[17]Tiwari, S., and Klar, A., "An Adaptive Domain Decomposition Procedure for Boltzmann and Euler Equations," *Journal of Computational and Applied Mathematics*, Vol. 90, 1998, pp. 223-237.
[18]Stewart, B. D., Pierazzo, E., Goldstein, D. B., Varghese, P. L., Trafton, L. M., and Moore, C. H., "Parallel 3D Hybrid Continuum/DSMC Method for Unsteady Expansions into a Vacuum," AIAA Paper 2009-266, 2009.
[19]Macrossan, M. N., "The Equilibrium Flux Method for the Calculation of Flows with Non-equilibrium Chemical Reactions," *Journal of Computational Physics*, Vol. 80, 1989, pp. 204-231.
[20]Burt, J. M., and Boyd, I. D., "A Low Diffusion Particle Method for Simulating Compressible Inviscid Flows," *Journal of Computational Physics*, Vol. 227, 2008, pp. 4653-4670.
[21]Burt, J. M., and Boyd, I. D., "Extension of a Multiscale Particle Scheme to Near-Equilibrium Viscous Flows," *AIAA Journal*, Vol. 47, No. 6, 2009, pp. 1507-1517.
[22]Burt, J. M., and Boyd, I. D., "A Hybrid Particle Approach for Continuum and Rarefied Flow Simulation," *Journal of Computational Physics*, Vol. 228, 2009, pp. 460-475.
[23]Burt, J. M., and Boyd, I. D., "Application of a Multiscale Particle Scheme to High Altitude Rocket Exhaust Flows," AIAA Paper 2009-1567, 2009.
[24]Burt, J. M., and Boyd, I. D., "Rotational and Vibrational Nonequilibrium in a Low Diffusion Particle Method for Continuum Flow Simulation," AIAA Paper 2009-3743, 2009.
[25]Sun, Q., and Boyd, I. D., "Evaluation of Macroscopic Properties in the Direct Simulation Monte Carlo Method," *Journal of Thermophysics and Heat Transfer*, Vol. 19, No. 3, 2005, pp. 329-335.
[26]Vincenti, W. G., and Kruger, C. H., *Introduction to Physical Gas Dynamics*, Krieger Publishing Company, Malabar, Florida, 1986.
[27]Bird, G. A., *Molecular Gas Dynamics and the Direct Simulation of Gas Flows*, Clarendon Press, Oxford, 1994.
[28]Laney, C. B., *Computational Gasdynamics*, Cambridge University Press, 1998.

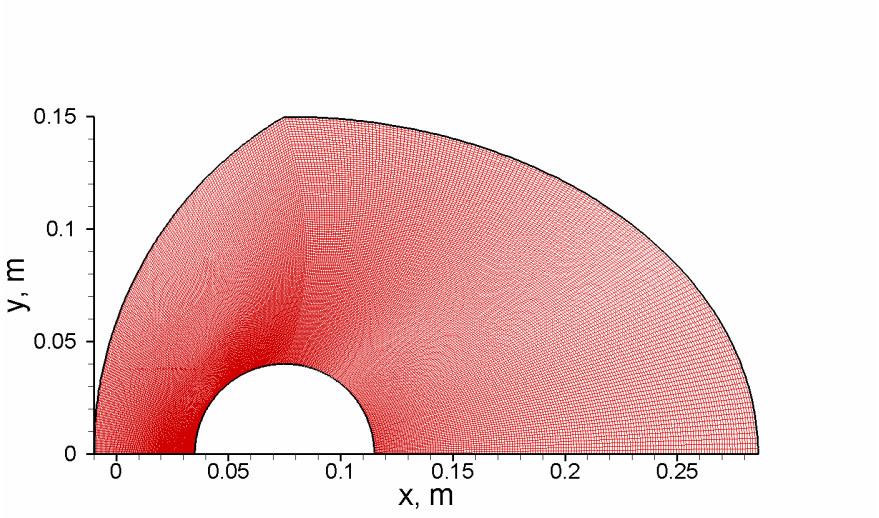

Figure 1. Computational mesh.

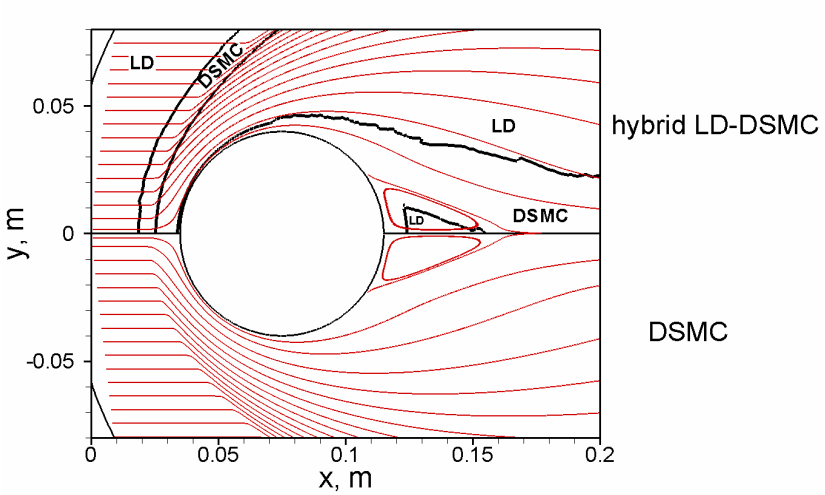

Figure 2. Streamlines and LD/DSMC domain boundaries. Hybrid simulation results are shown in the upper half of the figure, and streamlines from a DSMC simulation are in the lower half.

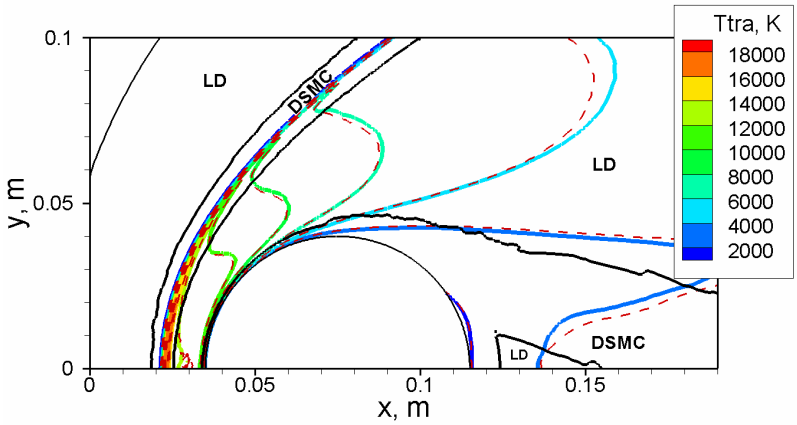

Figure 3. Contours of translational temperature from the hybrid LD-DSMC simulation and the DSMC simulation. Dashed lines indicate DSMC simulation results.

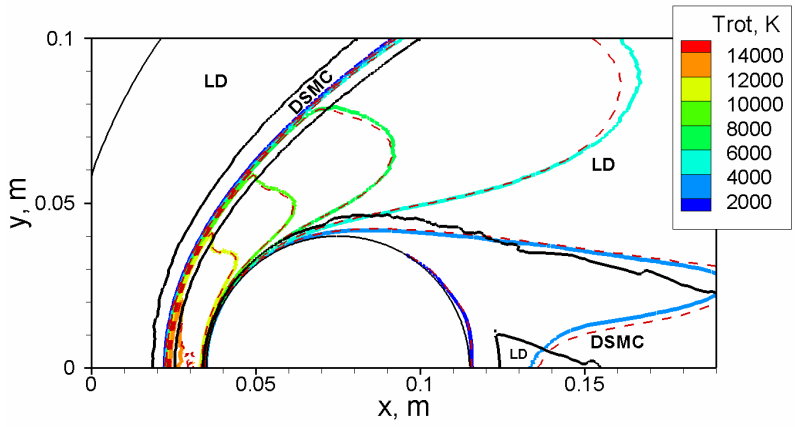

Figure 4. Contours of rotational temperature.

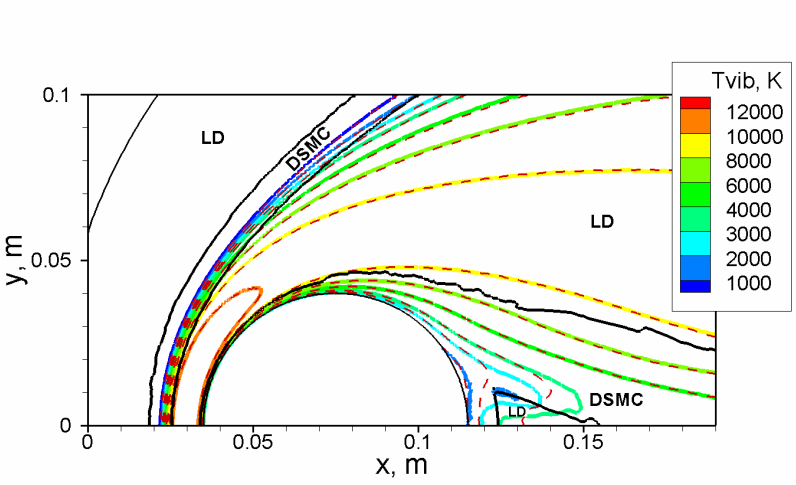

Figure 5. Contours of vibrational temperature.

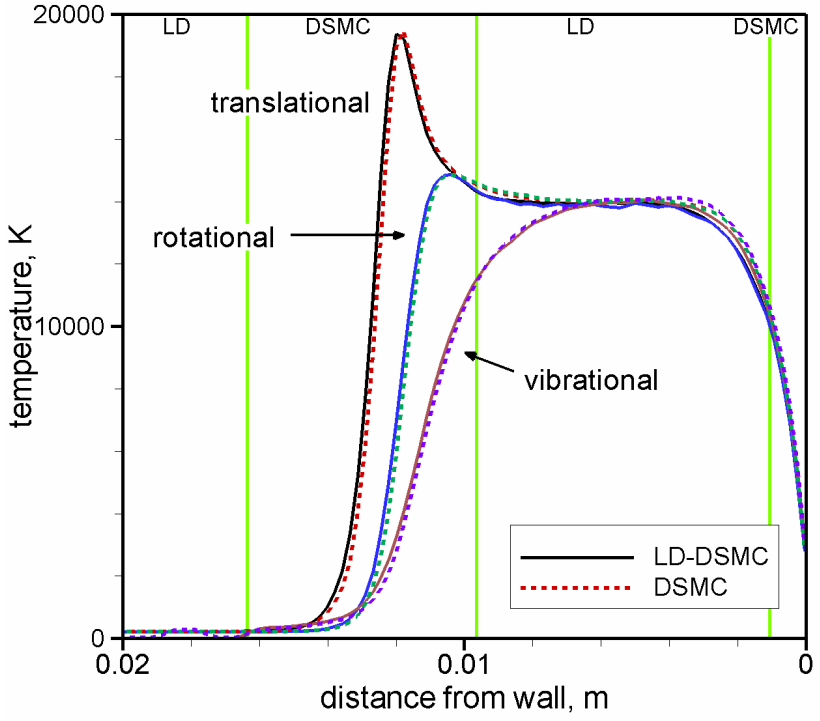

Figure 6. Variation in translational, rotational and vibrational temperatures along the stagnation streamline.

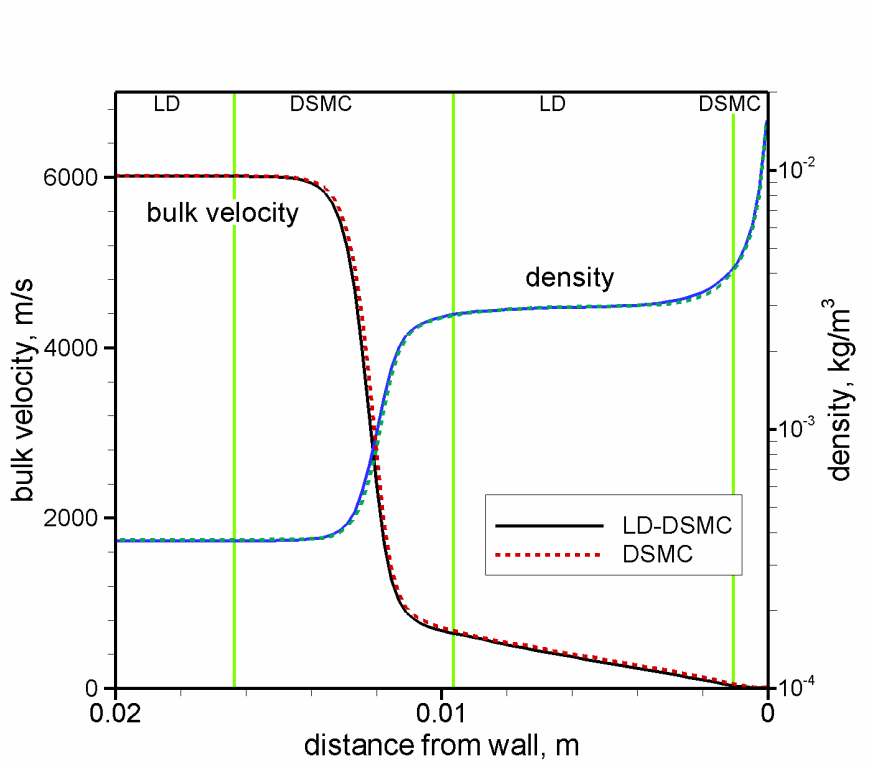

Figure 7. Variation in bulk velocity magnitude and density along the stagnation streamline.

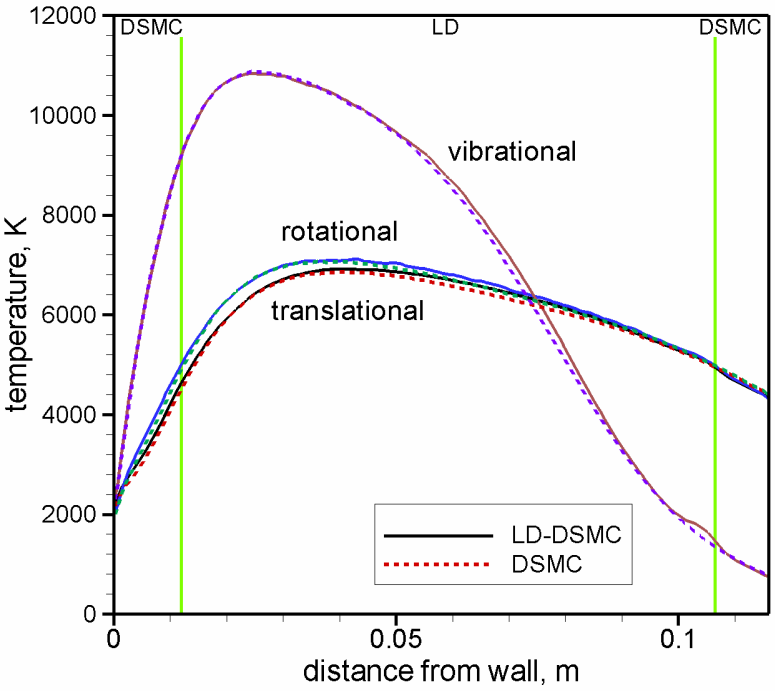

Figure 8. Variation in translational, rotational and vibrational temperatures along an extraction line inclined 60° from the freesteam direction.

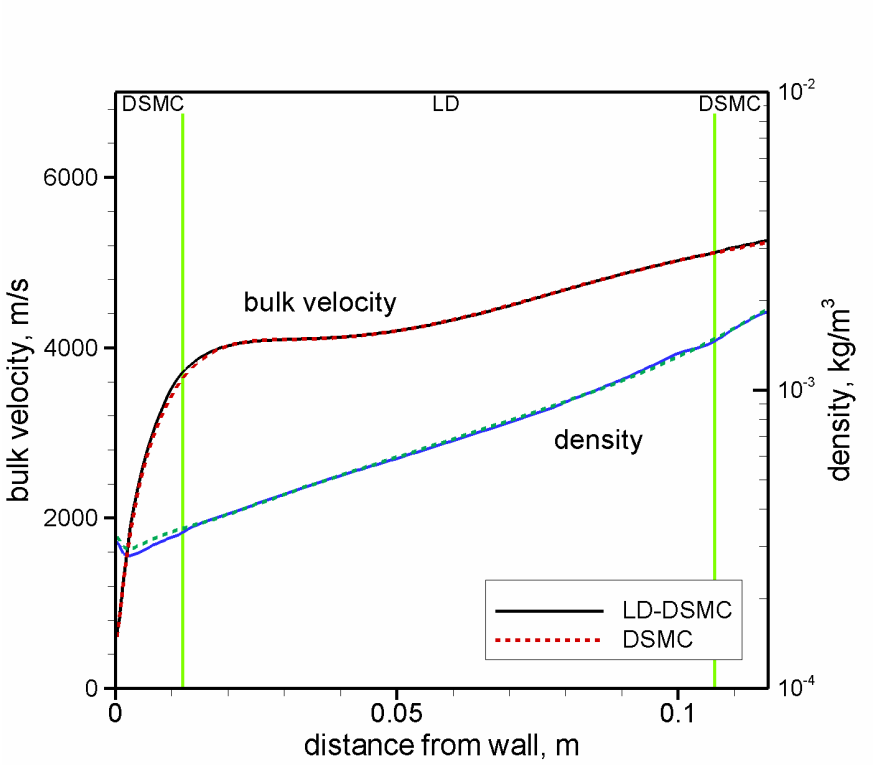

Figure 9. Variation in bulk velocity magnitude and density along the same extraction line as in Fig. 8.

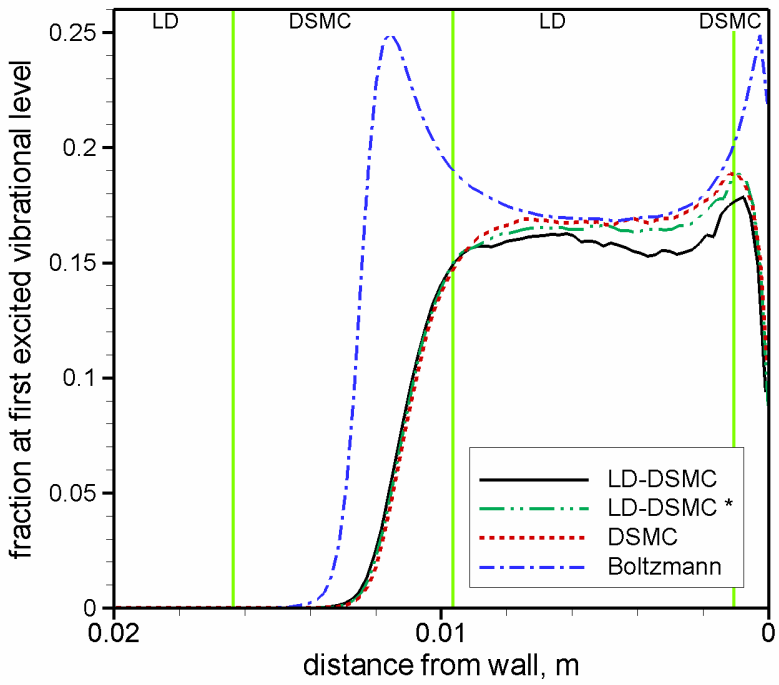

Figure 10. Variation along the stagnation streamline in the fraction of molecules at the first excited quantum vibrational energy level.